

Article

# Towards an *app* to estimate patient-specific perioperative femur fracture risk

V. Minutolo<sup>1</sup>, L. Esposito<sup>1</sup>, P. Gargiulo<sup>3</sup> and M. Fraldi<sup>2</sup>

<sup>1</sup> Department of Engineering, University of Campania “Luigi Vanvitelli”, Aversa (CE), Italy

<sup>2</sup> Department of Structures for Engineering and Architecture, University of Napoli Federico II, Napoli, Italy

<sup>3</sup> Institute for Biomedical and Neural Engineering, Department of Science, Landspítali University Hospital, University of Iceland, Reykjavik, Iceland

\* Correspondence luca.esposito@unina.it; (L.E.)

**Abstract:** Total Hip Arthroplasty is one of the most successful surgery. However, due to the worldwide growing population life expectancy and the related incidence of age-dependent bone diseases, a growing number of cases of intra-operative fractures lead to revision surgery with high rates of morbidity and mortality. Surgeons choose the type of the implant, either cemented or cementless prosthesis, on the basis of the age, the quality of the bone and the general medical conditions of the patients. Generally, no quantitative measures are available to assess the intra-operative fracture risk. Consequently, the decision-making process is mainly based on medical operators' expertise and qualitative information obtained by imaging. Motivated by this scenario, we here propose a mechanical-supported strategy to assist surgeons in their decisions, by giving intelligible maps of the risk fracture which take into account the interplay between actual strength distribution inside the bone tissue and its response to the forces exerted by the implant. To this end, we produce charts and patient-specific synthetic “traffic-light” indicators of fracture risk, by making use of ad hoc analytical solutions to predict the stress levels in the bone by means of CT-based mechanical and geometrical parameters of the patient. We felt that, if implemented in a friendly software or proposed as an app, the strategy could constitute a practical tool to help the medical decision-making process, in particular with respect to the choice of adopting cemented or cementless implant

**Keywords:** Total hip arthroplasty; intra-operative femur fracture risk; bone elastic-plastic behavior

## 1. Introduction

Total hip arthroplasty (THA) is one of the most successful orthopedic procedures with effective results in terms of durability and improvement in the quality of life [1]. However, perioperative periprosthetic femur fracture (PPF) after THA is a rare but devastating complication, with higher rates of morbidity and mortality.

Generally, PPFs occur during the surgical implantation of the prosthesis as a consequence of the induced mechanical stress by the stem insertion [2]; moreover, in the majority of the cases, the fracture is recognized after some time elapse only. In [3], it is reported that there is experimental evidence that the incidence of perioperative prosthetic femur fractures ranges from 0.3 to 27.8% in patients with cemented femoral components, and 2.95% to 27.8% in patients with cementless femoral components, such an incidence being independent on the age or sex of the patients as reported by Adel et al. [4].

Typically, when a cementless stem is implanted, the fracture events occur during femoral canal broaching or implant insertion while trying to obtain a tight press fit [5]. Cracks in the proximal femur due to press-fit stem implantation are often recognized only after surgery when patients already have

started to mechanically load their prosthesis [6]. It remains unclear which patient-dependent and/or hospital-dependent factors predispose to PPF after primary THA [7].

Due to the reflections above, and considering the evidence, surgeons usually rely on their experience since they do not have the support of quantitative mechanical measures for their decision-making process [8-10]. Generally, it reduces to a conservative choosing option: "older and less-healthy" patients receive cemented implants while for "younger and healthier" are preferred uncemented prostheses [11].

Although the fracture is a mechanical problem, while the literature is rich of works oriented to reduce the stress levels within the bone during the post-operative life of the implant through different optimization strategies [12-16], the intra-operative risk of PPF is poorly studied, at least in terms of outcomes to be directly adopted by surgeons. Malekmotiei et al. [17] propose an analytical approach to study the interference fit problem of the femoral stem in cementless THA. Esposito et al. [18] propose a numerical-based patient-specific strategy to estimate the risk of intra-operative PPF. To simulate the actual press-fitting phenomenon (i.e. the interaction between prosthesis and femur), a volumetric expansion of the broach volume was considered, since the female volume inside the femur is smaller than the male volume of the prosthesis. This expansion was obtained by applying a fictitious uniform variation of temperature to the broach nodes. The presented FE model refers to a patient-specific CT reconstruction that is very expensive in terms of human time to build up the geometry, to characterize the mechanical properties of the femur and to evaluate a priori ratios between geometrical and thermo-mechanical parameters [19], and in terms of computational time for meshing, preventing singularities due to the automatic model reconstruction [20] and solving the structural problem. The solutions obtained by computational mechanics are very useful to get scientific insight on the behaviour of the implants and to interpret the experimental evidence, but it is rather cumbersome to be used as a light and quick tool for intraoperative assistance to the surgeon's decision. With the aim scope of obtaining a patient-specific evaluation, it is mandatory that the mechanical data, concerning bone density and shape could be inputted in a straight forward way. Moreover, it is desirable that the analysis is completed in a few minutes.

In the present work, a simplified model is solved for evaluating the mechanical stress the bone tissue suffers during hip prosthesis implant. The results have been compared to those obtained from FEM analysis by Esposito et al. [18]. The procedure is based on an approximate model that consists of a plane representation of the femur cross-section. The shape of the cross-section is approximated by two concentric circular annuli made of two materials, a cortical type material at the outer portion of the annulus and a trabecular type material at the inner part. This approximation was used to calculate the analytical solution of the implant of a prosthesis stem modeled as applied radial displacement constraints. The approximate model allows calculating the structural response analytically, in this way it is possible to get the approximate strain distribution within the model quite immediately once the geometry, the material properties, and the applied constraints have been prescribed. Such a calculation based on a few simple parameters can be assumed as the base of the decision-making process in the intra-operative environment. To this aim, the used approach bases on the limit analysis methodology that ascribes the structural collapse to the fulfilment of limit condition for the material in conjunction with the suitable distribution of limit zones within the structure. When the material of the inquired bone reaches the assumed limit in a point, indeed, the structure does not collapse provided the overstress could transfer to the material in the vicinity. The collapse occurs only when no possible distribution of stress exists that is able to respect both equilibrium and limit compatibility [21-22]. In the work, mechanical compatibility is defined through the von Mises measure of strain. The implant is assumed to produce monotonically increasing radial displacement at the interface with trabecular bone tissue, in an essentially plane strain state. It is then considered that the strain, rather than the stress could be a good parameter of strength. Moreover, the deviatoric measure of the stress seems in the first approximation to give better results than spherical based measures. However, the introduction of different strain measures as limit parameter can be introduced without significant modification of the application. The criteria in terms of stress and strain coincide in the case of a monotone load path and the plane strain corresponding to vanishing

out of plane strain is completely described by the 2D model. This is not true for the stress that has a normal component that cannot be neglected and should be considered if a stress measure would be adopted as a limit parameter. Finally, literature data concerning bone resistance are mainly proposed in terms of limit strain that results from experimental analysis [23-24]. Starting from the considerations and the hypotheses above, the closed-form solution of the simplified model is obtained starting from the data constituted by the bone section characterization deriving from CT from the patient that furnishes the tissue density and the characteristic radius of the bone sections. Finally, the radius of the inner hollow and of the stem suggest the displacement constraints be applied as loading. The stress and the strain distribution are calculated by acquired CT data. The stress and strain distributions so determined were expressed in the form of a traffic color lights code in order to furnish direct and concise information to the medical operators. The assumed criterium was that, starting from the fact that in the neighbourhood of the implant the strain will always reach the limit but this is not a condition of collapse, the fracture risk increase if the overstrained zone approaches the cortical zone that has to be preserved in order to prevent bone failure. Hence, in the simplified criterion we have three possibilities: when the cortical zone appeared to have the strain level under the elastic limit, i.e. yield strain, the fracture risk is assumed to be null, when it presented the strain measure laying between the yield and the ultimate limit the fracture risk factor is considered low, finally, when the cortical zone strain measure is completely over limit, the fracture risk is high.

In the following, the procedure was described starting from the formulation of the mechanical problem of a two-phase hollow cylinder loaded by applied prescribed displacement on the inner boundary. The constraint simulated the action produced by the insertion of the stem of the prosthesis into the femur. The material phases were constituted by cancellous and cortical materials whose mechanical parameters depended on CT numbers. The structure was analytically calculated, the von Mises strain was evaluated and compared with the yield and ultimate limit of the material. The results were compared with some actual patients' case studies confirming the proposed prediction of the Fracture Risk. In conclusion, the methodology provided direct and easy to interpret results that could be the basis on which founding the decision-making process on the typology of the prosthesis to implant. The measures, deriving from actual patient CT, allowed considering the methodology as a patient-specific method for the prediction of the intra-operative femur fracture risk.

## 2. Materials and Methods

In this section, the novel analytical solution of a piecewise homogeneous annulus subjected to applied displacement constraints has been presented. The analytical solution has been used as a simplified model of the behaviour of a femur section during the hip prosthesis implant. The hypotheses of the model are plane strain and piecewise constant homogeneous elastic material that simulate heterogeneity of bone tissue. More accurate description is possible using Functional Graded Materials where graded transition can be obtained [25].

In order to study the interaction between the prosthesis and the bone tissue by means of an analytical approach that overcome the difficulties and the computational effort due to large computational approaches, the femoral diaphysis was modeled as a biphasic hollow cylinder (Figure 1 left).

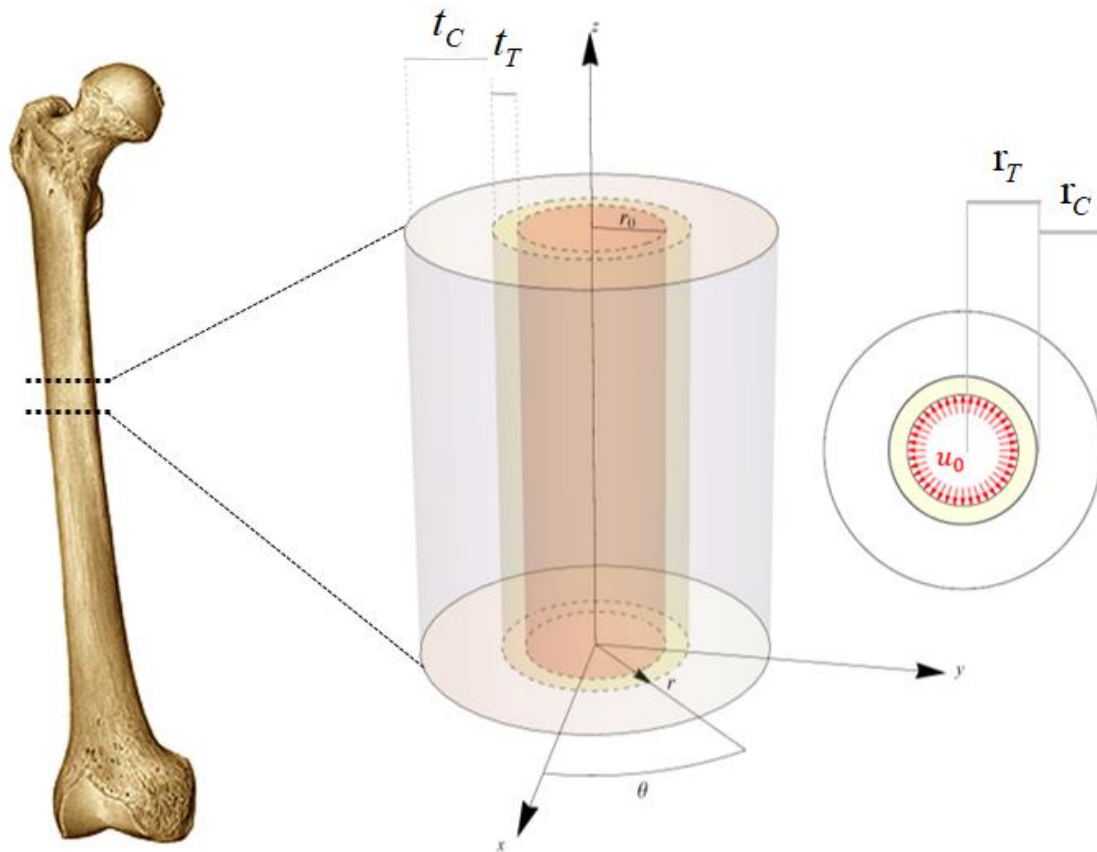


**Figure 1.** Three-dimensional model of the femoral diaphysis in cylindrical coordinates system (left). Cross-section of the model (right).

The internal cavity represented the diaphyseal canal, while the central and the external phases the trabecular and cortical bone, respectively. The only geometrical parameter of the model is the radius of the generic annulus, the bone regions have been described by the geometric loci whose definition inequalities are:

$$\begin{aligned}
 \text{Femoral Diaphysis} &: r \leq r_0, & 0 \leq \vartheta \leq 2\pi \\
 \text{Trabecular Bone} &: r_0 < r \leq r_T, & 0 \leq \vartheta \leq 2\pi \quad \text{with} \quad r_T = r_0 + t_T \\
 \text{Cortical Bone} &: r_T < r \leq r_C, & 0 \leq \vartheta \leq 2\pi \quad \text{with} \quad r_C = r_T + t_C
 \end{aligned} \tag{1}$$

where  $r_0$  is the internal radius,  $r_T$  and  $t_T$  are respectively the trabecular radius and the trabecular thickness and  $r_C$  and  $t_C$  denote the radius and the thickness of the cortical region.

The cancellous and the cortical bone tissues were supposed - at the macroscopic scale of interest - as overall isotropic and linear elastic materials [26]. However, the spatially inhomogeneous mechanical properties due to the different levels of bone mineral density were taken into account, averaging the actual stiffness and strength values over proper domains of the idealized hollow bi-phase cylinder, denoting trabecular and cortical bone tissue elastic moduli, densities, yield and ultimate strains, respectively as  $E_T$ ,  $\rho_T$ ,  $\varepsilon_y^T$ ,  $\varepsilon_{ult}^T$  and  $E_C$ ,  $\rho_C$ ,  $\varepsilon_y^C$ ,  $\varepsilon_{ult}^C$ . Poisson coefficients were indicated as  $\nu_T$  and  $\nu_C$ , assuming  $\nu_T = \nu_C$ .

In the case of THA without the use of the cement, in order to reach the press-fit of the prosthesis into the femur, the stem component volume results generally 10% greater than the volume prepared by the surgeon in the diaphysis canal. For this reason, due to the insertion of the prosthesis, the stem component is forced to occupy the undersized surgically prepared volume into the femoral

diaphysis, by pressing on the surrounding bone tissue by a prescribed radial displacement, namely  $u_0$  (Figure 1 right).

With the aim of simulating this scenario, a linear elastic analysis was carried out in the hypothesis of small displacements through an analytical procedure implemented in the software Mathematica® (Wolfram Research, 2019). By using a cylindrical reference system  $(r, \theta, z)$ , the kinematics of the problem was described by means of the following displacement field

$$\mathbf{u}^k = (u_r^k, u_\theta^k, u_z^k) \quad (2)$$

with

$$\begin{aligned} u_r^k &= u^k(r) \\ u_\theta^k &= 0 \\ u_z^k &= \varepsilon_0 z \end{aligned} \quad (3)$$

$u_r^k, u_\theta^k, u_z^k$  denoting respectively the radial, circumferential and longitudinal components of the displacement, and the apex  $k = \{T, C\}$  referring to the bone tissue type ( $T$ : trabecular,  $C$ : cortical).

The strain tensor was expressed in the Voigt's notation

$$\boldsymbol{\varepsilon}^k = (\varepsilon_{rr}^k, \varepsilon_{\theta\theta}^k, \varepsilon_{zz}^k, \varepsilon_{r\theta}^k, \varepsilon_{rz}^k, \varepsilon_{r\theta}^k) = \left( \frac{du_r^k}{dr}, \frac{u_r^k}{r}, \varepsilon_0, 0, 0, 0 \right) \quad (4)$$

being  $\varepsilon_{rr}^k = \frac{du_r^k}{dr}$  the radial strain,  $\varepsilon_{\theta\theta}^k = \frac{u_r^k}{r}$  the circumferential strain and  $\varepsilon_{zz}^k = \varepsilon_0$  the longitudinal strain. In particular, the axial strain,  $\varepsilon_0$ , is considered constant and is calculated by means of equilibrium along the axis of the bone.

At any point of the bone, we asked the linear elastic constitutive equation to be valid and the cylindrical symmetry of the structure allows reducing the equilibrium equations to the sole one in the radial direction

$$\nabla \cdot \boldsymbol{\sigma}^k = 0 \quad (5)$$

By considering the stress-strain constitutive equation and the kinematical relationships recalled above, the following well-known equilibrium equation in term of displacements can be written down

$$\frac{d\sigma_{rr}^k}{dr} + \frac{1}{r}(\sigma_{rr}^k - \sigma_{\theta\theta}^k) = 0 \quad (6)$$

whose solution is given in the form

$$u_r^k = C_1^k r + C_2^k r^{-1} \quad (7)$$

The integration constants  $C_1^k$  and  $C_2^k$  were determined by imposing the boundary and interface conditions, namely

- Boundary conditions

$$\begin{aligned} r = r_0 : u_r^T(r_0) &= u_0 \\ r = r_C : \sigma_{rr}^C(r_C) &= 0 \end{aligned} \quad (8)$$

- Interface conditions

$$\begin{aligned} r = r_T : \sigma_{rr}^T(r_T) &= \sigma_{rr}^C(r_T) \\ u_r^T(r_T) &= u_r^C(r_T) \end{aligned} \quad (9)$$

For both the phases, the radial displacements  $u_r^k(r)$  were obtained, their expressions being explicitly reported below ( $\nu = \nu_T = \nu_C$ )

$$u_r^T(r) = \frac{[r_C^2 + r_T^2(1-2\nu)]\{r_i r_T^2(u_0 + r_i \epsilon_0 \nu) + r^2[r_T^2 \epsilon_0 \nu + r_i u_0(1-2\nu)]\} E_T + (r_C - r_T)(r_C + r_T)(1-2\nu)[r_i r_T^2(u_0 + r_i \epsilon_0 \nu) - r^2(r_i u_0 - r_T^2 \epsilon_0 \nu)] E_C}{r(r_C - r_S)(r_C + r_T)(-r_i + r_T)(r_i + r_T)(-1+2\nu) E_C - r[r_S^2 + r_i^2(1-2\nu)][r_C^2 + r_S^2(1-2\nu)] E_T} \quad (1)$$

$$\begin{aligned} u_r^C(r) &= \frac{(1+\nu)\{2r_C^2 r_i r_T^2(\nu-1)(u_0 + r_i \epsilon_0 \nu) + r^2[r_T^2 \epsilon_0 \nu(r_C^2 + r_T^2 - 2r_T^2 \nu) - 2r_i r_T^2 u_0(\nu-1)(2\nu-1) - r_i^2(r_C - r_T)(r_C + r_T)\epsilon_0 \nu(2\nu-1)]\} E_C}{r(1+\nu)\{(r_C - r_T)(r_C + r_T)(r_T - r_i)(r_i + r_T)(2\nu-1) E_C - [r_T^2 + r_i^2(1-2\nu)][r_C^2 + r_S^2(1-2\nu)] E_T\}} + \\ &+ \frac{r^2(r_C - r_T)(r_i - r_T)(r_C + r_T)(r_i + r_T)\epsilon_0 \nu(2\nu^2 + \nu - 1) E_C}{r(1+\nu)\{(r_C - r_T)(r_C + r_T)(r_T - r_i)(r_i + r_T)(2\nu-1) E_C - [r_T^2 + r_i^2(1-2\nu)][r_C^2 + r_S^2(1-2\nu)] E_T\}} \end{aligned} \quad (2)$$

Once the radial displacements were known, strain and stress components for each phase were derived. The flow-chart of the whole procedure is shown in Figure 2.

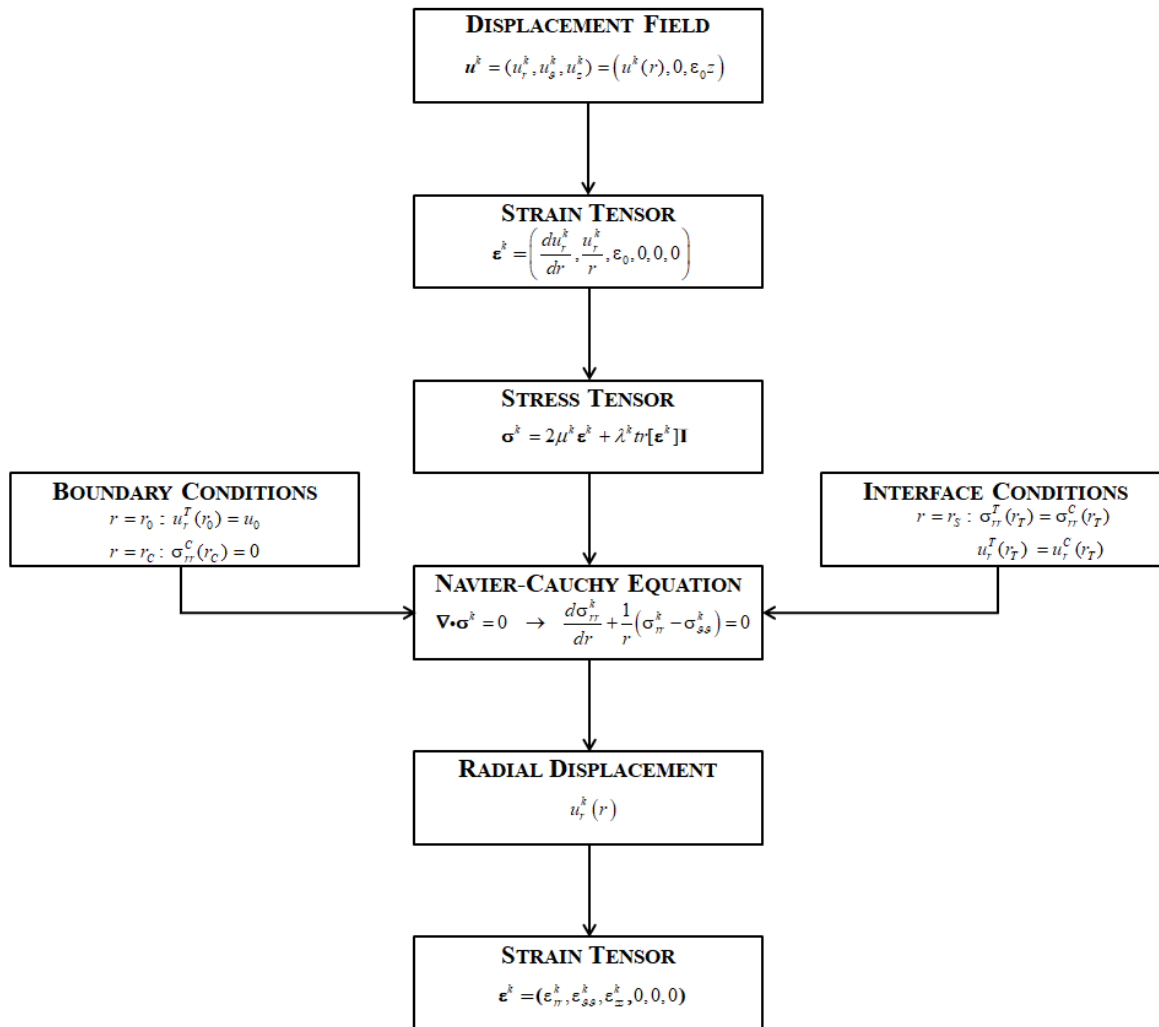


**Figure 2.** Flow-chart of the procedure.

The stress and strain components result only functions of  $r$ , the solution thus finally depending upon geometrical and constitutive properties of the two phases, as well as, on the prescribed radial displacement  $u_0$ , here representing the effect of the insertion of the prosthesis.

### 2.1. Evaluation of the patient-oriented material properties

In order to derive the mechanical properties of the bone from patient data records, the same scheme proposed by Esposito et al. [18] was utilized. The method consisted of the following steps: the bone material properties were estimated from the CT scan data, firstly converted into apparent bone densities,  $\rho_{app}$ , by using a phantom calibration; then, the value of ash density,  $\rho_{ash}$ , was obtained from the apparent density. Finally, in order to get the actual material properties, the Young's Modulus,  $E$ , of the bone tissue was related to the ash density [27].

### 2.2. A straight definition of Fracture Risk Factor (FRF)

A simple and direct estimation of the parameter that defines the fracture risk during the implant is described hereafter. As a measure of the material behavior, in literature both stress and strain levels within the bone were considered [28-31]. In this work, as a measure a measure of Fracture Risk Factor, the von Mises equivalent strain was calculated and compared with the admissible values from the literature.

In particular, the equivalent strain was compared to the yield and the ultimate strain. In detail, it was assumed that the yield strain was 0.0069 [23] and the ultimate strain 0.0145 [24] for both tissue. The assumed criterion for evaluating the risk factor is therefore set as follows:

Preliminary classification of the strain level used for defining the admissibility strain domain:

Level 1.  $\varepsilon_{vM}(r) \leq \varepsilon_Y$ , the bone tissue is safe;


Level 2.  $\varepsilon_Y < \varepsilon_{vM}(r) < \varepsilon_{ult}$  the bone tissue has to be considered yielded but not crashed;

Level 3.  $\varepsilon_{ult} < \varepsilon_{vM}(r)$  the bone tissue is crashed.

The admissibility domain constitutes the set of admissible solutions for local strain and should be integrated into global structural behaviour considering the collapse mechanism corresponding to the typical PPFs [32]. In the actual proposed procedure, the PPF is considered to occur when the over yield strain extends from the inner constrained boundary through the tissue and reaches the cortical bone. Finally, as the Fracture Risk, (FR) factor, the level of the cortical bone strain has been considered, namely: when the Level 3 of the strain involves completely the tissue up to the cortical zone the Fracture Risk is considered at a high level, when the cortical bone strain belongs to Level 2 the Fracture Risk has to be considered moderate, when the cortical tissue strain belongs to Level 1 the bone can be assumed having a low fracture risk.

The above-mentioned procedure was applied to the slices located at the middle of each Gruen Zones [33], and the obtained FR classification was expressed through a simple and intelligible “traffic lights” color code in order to provide immediate and concise information to surgeons. In other words, the obtained results were plotted along the radius, and colored in green indicating the strain belonged to Level 1, in orange Level 2 and in red Level 3. Moreover, colored plots of the sections were shown in order to provide direct and concise information to the medical operators. We refer to this depiction scheme as “Fracture Risk Factors” (Table 1).

**Table 1.** Traffic Lights Color Code.

VON MISES STRAIN	FRACTURE RISK FACTORS	TRAFFIC LIGHTS COLOR CODE
$\varepsilon_{vM} > \varepsilon_{ult}$	HIGH RISK OF FRACTURE	
$\varepsilon_Y < \varepsilon_{vM} < \varepsilon_{ult}$	LOW RISK OF FRACTURE	
$\varepsilon_{vM} < \varepsilon_Y$	SAFE	

### 2.3. Sensitivity analysis

As a first application, a sensitivity analysis has been performed by applying increasing constraints on the inner boundary of the structural section and evaluating the strain and its spreading within the tissue. The reference section was the central section of the Gruen Zone 1. The Zone is situated in the proximal region of the femur where the fractures' phenomena are typically located. The material properties and the geometry of the sample specimen were obtained from a young patient [34]; the case studied represents a typical reference in terms of material densities and constitutive properties for a successful surgical scenario. The cortical and the trabecular radii were  $r_t = 21mm$  and  $r_c = 18mm$ , moreover the Young moduli were set equal to  $20000MPa$  and  $4000MPa$  for the cortical and trabecular tissue. The moduli correspond to apparent densities of



$2 \frac{g}{cm^3}$  and  $0.7 \frac{g}{cm^3}$ , respectively. The yield strain was  $\varepsilon_y = 0.0069$  [34] and the ultimate strain  $\varepsilon_{ult} = 0.0145$  [24] for both tissue. The radius of the prosthesis was  $r_0 = 8.5mm$ , and the prescribed displacement,  $u_0$ , producing a volumetric increment equal to 10%, was  $u_p = 0.4683mm$ . The data of the analysis were collected in Table 2.

**Table 2.** Constitutive and geometrical properties of the trabecular and cortical bone tissue at the central section of the Gruen Zone 1.

	Cortical Tissue	Trabecular Tissue
Radius [mm]	21	18
Young Modulus [Mpa]	20 000	4 000
Poisson's Coefficient	0.4	0.4
Density [g/cm <sup>3</sup> ]	2.0	0.7
Yield Strain	0.0069	0.0069
Ultimate Strain	0.0145	0.0145

	Prosthesis
Radius [mm]	8.5
Prescribed displacement [mm]	0.4683

For the analysis of the sensitivity of the formulation, the components of the stress and strain (radial, circumferential, longitudinal and von Mises's) were calculated for trabecular and cortical phases. The analytical approach allows computing what applied constraint, in terms of prescribed boundary displacement, one should apply for obtaining prescribed von Mises strain distribution. In particular, it was possible to define two different displacement constraints for each bone tissue zones, i.e.

$$\left. \begin{array}{l} u_Y^k : \varepsilon_{vM}^k = \varepsilon_Y \\ u_{ult}^k : \varepsilon_{vM}^k = \varepsilon_{ult} \end{array} \right\} k = C, T \quad (3)$$

That was the constraint values producing, at the very first single point of the slice, the yield or the ultimate von Mises strain in the cortical, superscript C, or the trabecular, superscript T, zone.

In the analysed case the results were:

$$u_Y^T = 0.0480 \text{ mm}; u_{ult}^T = 0.1010 \text{ mm}; u_Y^C = 0.2430 \text{ mm}; u_{ult}^C = 0.5107 \text{ mm} \quad (4)$$

The sensitivity analysis consisted in applying constraint displacements varying from  $u_Y^T$  to  $u_{ult}^C$ . The resulting strain within the slice has resulted to vary with the radius decreasing when one moves from the center to the external cortex.

### 3. Results

In order to evaluate the reliability of the proposed analytical procedure, preliminary sensitivity analyses were performed by varying the magnitude of the prescribed radial displacements. The

sensitivity analysis showed that the strain depends on the distance from the inner hole, where the implant has been inserted. Moreover, the strain decreases rapidly from the inner stem surface toward the bone cortex. The behavior of the strain allows us to consider that the inmost tissue, subjected to the effect of stem implant will undergo severe values of strain that decreases with an almost exponential way. The high strain level does not represent the indicator of collapse, say fracture, but a local crisis that is almost inevitable. It has to be stressed that the collapse occurs when the strain overcame the yield limit in an entire portion of the structure till cortex. It is thus to consider that it is impossible that the strain in the neighborhood of the stem is under the yield value but this will not affect the prosthesis safety during daily activities.

It is worth to highlight that the displacement producing the limit value in the cortical phase,  $u_Y^C$ , was more than two times greater than the prescribed displacement producing the ultimate strain in the trabecular tissue,  $u_{ult}^T$ , as well as we found that  $u_{ult}^C \approx 5u_{ult}^T$ . In other words, the prescribed displacement  $u_0^{PRO}$  due to the insertion of the stem component - assumed to be  $u_0^{PRO} = 0.4683mm$  - produces strains which overcome the elastic limits of both cortical and spongy bone, while the ultimate strain is attained and overcome only in the trabecular region. This means that the cortical tissue did not undergo permanent strain and, even if high stress levels tend to approach the material threshold, no failure is therein expected, while trabecular tissue appears as at high fracture risk level.

As mentioned above, in the sensitivity analysis, several values of displacements at the innermost surface,  $u_0$ , were prescribed, running from  $u_Y^T$  to  $u_{ult}^C$ . The obtained results, in terms of strains versus bone radius, are shown in Figure 3, where the red and green horizontal lines are drawn at the yield and ultimate level, allowing to evaluate the position along the radius where the strain overcomes the thresholds.

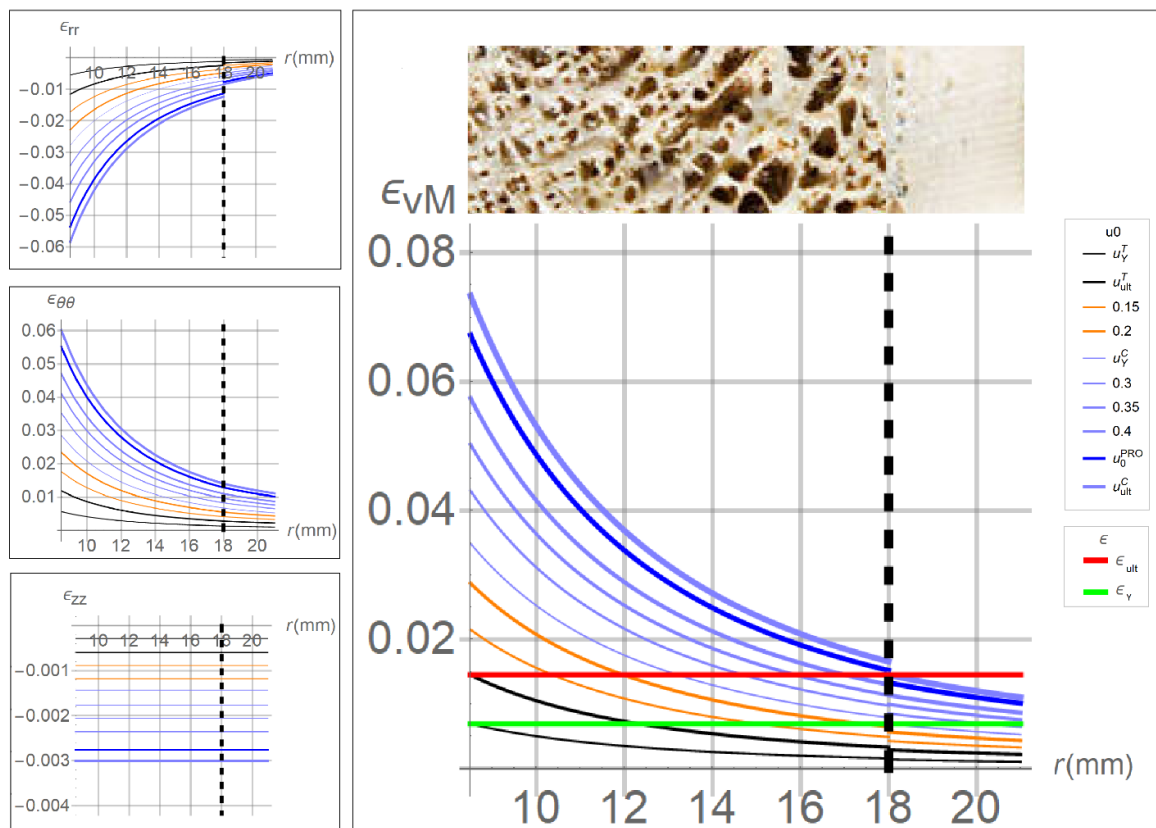


**Figure 3.** Distribution of radial (upper left), circumferential (middle left), longitudinal (lower left) and Von Mises strain (right). The black curves refer to the displacement that produces the strain between yield and ultimate values in the cortical annulus, the orange curves describe the strain produced by displacement that causes the strain between the ultimate and the yield values for respectively trabecular and cortical tissues, the light blue indicates the strain in the range between the yield and

the ultimate values within the cortical bone, boldface blue line denoting the effect of the displacement due to the insertion of the stem.

In particular, when the prescribed displacements  $u_0$  was less than  $u_Y^T$ , the whole bone strain was contained below the elastic limit and hence the tissue can be assumed to be safe. When  $u_0$  was between  $u_Y^T$  and  $u_Y^C$ , the von Mises strain in the trabecular tissue exceeded the ultimate value indicating the tissue is overstressed at the same time, the cortical tissue was completely preserved.

The strain components in the cylindrical reference are depicted on the left of Figure 3. It can be noted that the main contribution to von Mises strain,  $\varepsilon_{vM}^k$ , was given by the in-plane strains,  $\varepsilon_{\theta\theta}^k$  and  $\varepsilon_{rr}^k$ . Moreover, the axial strain,  $\varepsilon_{zz}^k$ , was one order smaller than the other components, and the radial strain,  $\varepsilon_{rr}^k$ , result negative since the compression due to the insertion of the prosthesis.

### 3.1. Comparison of the Fracture Risk Factor results obtained by means of the analytical and FEM approaches

In order to evaluate the feasibility of the proposed procedure, the data obtained from the CT scan of two patients before the surgery were utilized, the first suffered a fracture event during the implant and the second presented successful result. The CT data were used to obtain the mean value of the constitutive properties related to bone density. The shape of the bone was approximated to a hollow cylinder where the cross-section was assumed to have the same area of the actual one. The proposed analytical procedure was then applied to the two case studies and the FRF values were calculated. The results were compared to those obtained by means of FEM approaches from Esposito et al. [18].

For both patients, three femoral sections, proximal, medial and distal, were selected in the middle of each Gruen zone, and the analytical analyses were performed by setting the average geometrical and constitutive properties calculated from CT data for each section, listed in Table 3.

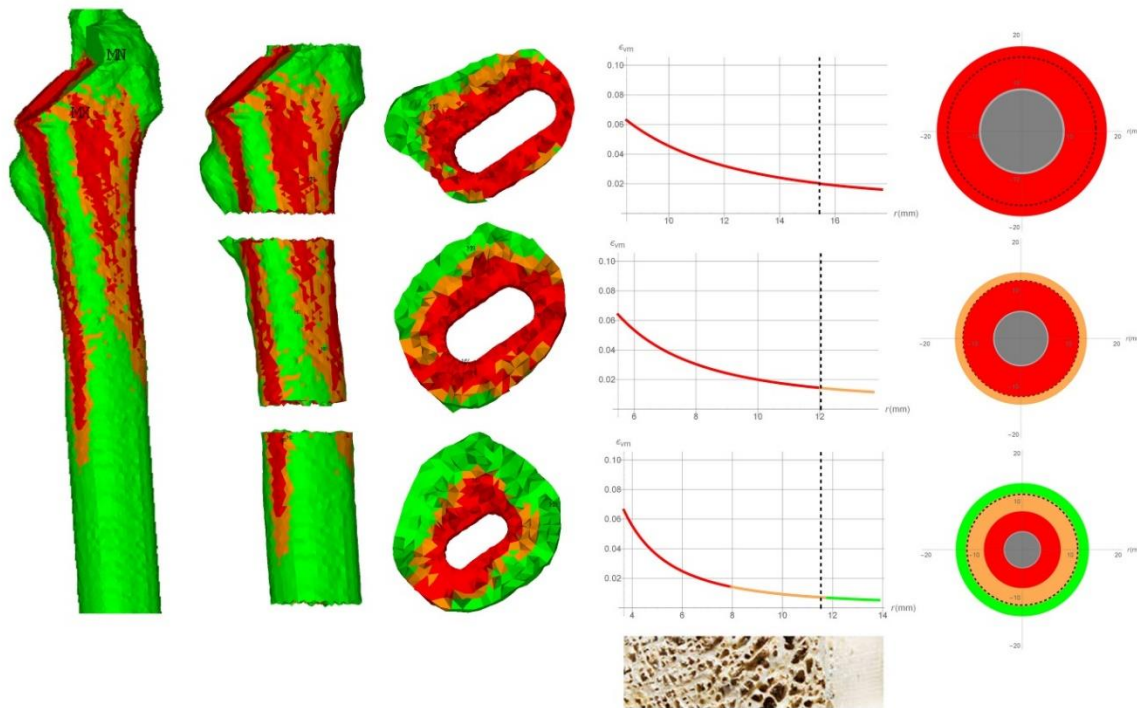
**Table 3.** Geometric and constitutive properties for fractured and un-fractured patients, obtained from CT data.

Fractured Patient						
Cortical bone		Trabecular bone		Prosthesis		
Slice	Young Modulus [MPa]	Radius [mm]	Young Modulus [MPa]	Radius [mm]	Radius [mm]	Prescribed Displacement [mm]
Proximal	6784.2852	17.6796	4799.6436	15.4339	8.4708	0.4666
Medial	8166.8600	13.7304	7438.5087	12.0371	5.4743	0.3016
Distal	8288.6042	13.8508	7516.2335	11.5322	3.6661	0.2020

Un-Fractured Patient						
Cortical bone		Trabecular bone		Prosthesis		
Slice	Young Modulus [MPa]	Radius [mm]	Young Modulus [MPa]	Radius [mm]	Radius [mm]	Prescribed Displacement [mm]
Proximal	7611.5127	21.2760	4715.3445	18.0206	8.4126	0.4634
Medial	8882.9168	15.5881	7927.6850	12.8490	5.5006	0.3030
Distal	9221.9785	14.1060	8680.2633	11.7860	3.6128	0.1990

The results for each Gruen Zone, related to the fractured patient, are illustrated in Figure 4.



**Figure 4.** (a) Fractured patient case; for each slice, located at the middle part of each Gruen zone, the FEM results (left), the trend of the von Mises strain along  $r$  (center), and FRF code (right).

On the left, the FEM results were shown as reported by Esposito et al. [18]. In the Figure middle, the von Mises strain was plotted along the radius and, on the right, the FRF was expressed in terms of traffic lights code, calculated by means of the analytical approach.

Subsequently, the results were compared to those from the literature [18]. In fact, in this cited study, a patient that underwent an intra-operative periprosthetic fracture and another with a successful outcome were recruited from a cohort of 36 patients undergoing primary THA. In the cited paper, the finite element analyses is performed in order to investigate the distributions of stress and strain inside the femur and to calculate the FRF. The results reported in Esposito et al. [18] were obtained by detailed geometric reconstruction of the femurs and the prosthesis. Moreover, the material properties have been described using non-linear behaviour considering elastic-plastic constitutive properties of the bone as a function of the local density. The results from the FEM analysis performed by Esposito et al. [18] have been used as a benchmark of the present analytical simplified calculations. The results related to the fractured patient were shown in Figure 4. The FEM output from Esposito et al. [18] is reported on the left. The strain maps are reported on the 3D model of the femur and showed that the proximal Gruen Zone 1-7 was interested by strain that reaches the ultimate limit as it was highlighted by the wide red zone. It has to be stressed that the presence of the red zone within the great part of the cross-section especially with the high strained part of the bone that has reached the external geometrical boundary, can be assumed as an index of a high risk of fracture, a fact confirmed by the observation that the patient actually presented intraoperative fracture. Besides the FEM results, the actual calculation results are represented as a strain diagram versus the radius of the section of the bone. It can be seen that, even with the simplified approach, a high risk of fracture was evaluated for the proximal section of the femur. In fact, the von Mises strain resulted greater than the ultimate strain value for the whole bone tissue. On the right, a schematic image of the cross-section was shown where a color code highlighted the FRF: therein, red saturated the section, this meaning that the bone district was subjected to high risk of fracture. In addition, it can be seen that in the Gruen zone 2-6, while the trabecular bone resulted at a high level of strain, in the cortical bone it was low hence it can be assumed that the risk of fracture in the zones is low as well. In the Gruen zone 3-5, the cortical bone resulted safe, while the trabecular bone presented a high

risk of fracture around the prosthesis and a low risk of fracture extending from the half part of the trabecular bone until the interface between trabecular and cortical bone.

The results related to the un-fractured patient were shown in Figure 5.

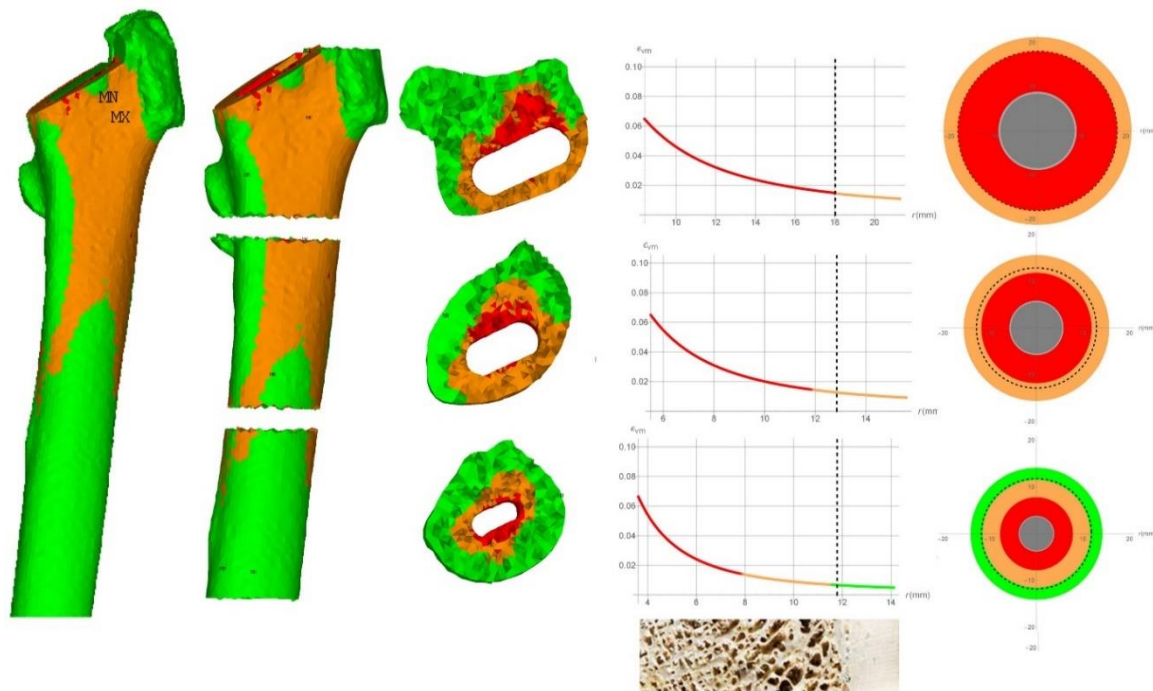


**Figure 5.** FRF maps from the FEM analysis (left) and the analytical procedure (right).

Also in this case, all the bone in contact with the prosthesis appeared to be red because the values of the von Mises strain were always greater than the ultimate one. The cortical bone resulted at a high strain level in the Gruen zone 1-7 and 2-6, while it results at a low strain level in Gruen zone 3-5. It is worth to be noted that in Gruen zone 2-6, the orange zone extended to part of the trabecular tissue, as confirmed by the FEM results. In this case, because the red zone did not reach the cortical bone, the patient can be considered to have further load-bearing capacity and therefore it can be supposed to host the implant without fractures.

Summing up, in both cases, the results obtained by the analytical procedure were similar to those achieved by the FEM analyses. In the case of the fractured patient, the results of the analytical procedure showed a red region with high fracture risk in both the trabecular and cortical tissue confined in the proximal section. In the case of an un-fractured patient, there was an orange area related to high strain although under the ultimate limit, in the proximal zone of the femur, located in the cortical tissue, all these outcomes being consistent with numerical simulations and clinical evidence.

#### 4. Conclusions

In this work, an analytical-based procedure is presented with the aim of predicting the intra-operative fracture risk in the case of THA in a direct, straightforward way. The methodology makes use of a simplified model to predict the mechanical interaction between the prosthesis and the femur bone, with the advantage of resulting in immediate, concise and intelligible maps of fracture risk which we felt, if implemented in a friendly code or as an app, could constitute a practical tool to help the medical decision-making process, in particular with respect to the choice of adopting cemented or cementless implant. The maps were expressed in term of traffic lights color code, obtained by transferring into a direct measure of fracture risk, based on the comparison between in situ von Mises strain and corresponding bone-dependent strain thresholds. The effectiveness of the proposed procedure was confirmed by comparing the obtained results in terms of strain with those from more

precise FE models. The strain calculation has been done with reference to two actual patient cases whose CT data were utilized to define geometrical and constitutive parameters. The obtained strain maps through the analytical formulation have been interpreted following the proposed criteria where red yellow and green zones have been used as a flag for fracture risk evaluation. In particular, the eventuality the red zone reached the cortical bone is assumed as a high fracture risk index. The strain level distribution has been checked by comparison with numerical calculation on a very accurate geometrical finite element model in the literature (Esposito et al.2018) that assumes a non-linear constitutive model of the bone tissue whose data are obtained by CT tests. It has to be stressed that the possibility of building up an accurate FE model and performing non-linear calculations has a very high cost in terms of computing time. To build up a 3D model of a femur with a usual PC from CT images and to perform calculation of non-linear model costs an order of magnitude time of days. The analytical approximate solution takes a few seconds.

The proposed methodology is able to provide direct information with a limited cost in terms of computational time and interpretation of the results. Due to the simplicity of the implementation, the methodology could be applied to different sections of the femur and extended to a multi-phase model - by dividing the section into more than two annuli - with no significant effort.

In conclusion, the analytical procedure has been shown that is able to furnish confident strain maps of the femur sections. The strain maps are quite comparable to more sophisticated numerical results in the sense to give global information on the possibility that the strain produced by the insertion of the prosthetic stem does involve the whole structural strength reserve of the bone cross-section..

**Author Contributions:** “Conceptualization, V.M., L.E., P.G. and M.F.; methodology, V.M., L.E., P.G. and M.F.; software, V.M., L.E., P.G. and M.F.; validation, V.M., L.E., P.G. and M.F.; formal analysis, V.M., L.E., P.G. and M.F.; investigation, V.M., L.E., P.G. AND M.F.; resources, V.M., L.E., P.G. AND M.F.; data curation, V.M., L.E., P.G. AND M.F.; writing—original draft preparation, V.M., L.E., P.G. AND M.F.; writing—review and editing, V.M., L.E., P.G. AND M.F.; visualization, V.M., L.E., P.G. AND M.F.; supervision, V.M., L.E., P.G. AND M.F.; project administration, V.M., L.E., P.G. AND M.F.; funding acquisition, V.M., L.E.. All authors have read and agreed to the published version of the manuscript.”, please turn to the [CRediT taxonomy](#) for the term explanation. Authorship must be limited to those who have contributed substantially to the work reported.

**Funding:** This research was funded by the Università degli Studi della Campania “L.Vanvitelli”, grant Programma VALERE: “VAnviteLli pEr la RicErca”, DDG n. 516 – 24/05/2018..

**Conflicts of Interest:** “The authors declare no conflict of interest.”

## References

1. Ethgen O, Bruyere O, Richy F, Dardennes C, Reginster JY. 2004. Health-related quality of life in total hip and total knee arthroplasty: a qualitative and systematic review of the literature. *J Bone Joint Surg Am.* 86:963-74.
2. Dumont GD, Zide JR, Huo MH. 2010. Periprosthetic femur fractures: Current concepts and management. *YSART* 21:9-13.
3. Mayle RE, Della Valle CJ. 2012. Intra-operative fractures during THA: see it before it sees us. *J Bone Joint Surg (Br).* 94:26-31.
4. Abdel M, Watts C, Houdek M, Lewallen D, Berry D. 2016. Epidemiology of periprosthetic fracture of the femur in 32 644 primary total hip arthroplasties: a 40-year experience. *Bone Joint J.* 98:461-7.
5. Holley K, Zelken J, Padgett D, Chimento G, Yun A, Buly R. 2007. Periprosthetic fractures of the femur after hip arthroplasty: an analysis of 99 patients *HSS J.* 3:190-197.
6. Savin L, Barharosie C, Botez P. 2012. Periprosthetic femoral fractures-evaluation of risk factors. *Rev Med Chir Soc Med Nat Iasi.* 116:846-852.
7. Thien TM, Chatziagorou G, Garellick G, Furnes O, Havelin LI, Mäkelä K, Overgaard S, Pedersen A, Eskelinen A, Pulkkinen P, Kärrholm J. 2014. Periprosthetic femoral fracture within two years after total hip replacement: analysis of 437,629 operations in the nordic arthroplasty register association database. *J Bone Joint Surg Am.* 96(19):e167.

8. Gargiulo P, Gislason MK, Edmunds KJ, Pitocchi J, Carraro U, Esposito L, Fraldi M, Bifulco P, Cesarelli M, Jónsson H. 2018. CT-based bone and muscle assessment in normal and pathological conditions. *Encyclopedia of Biomedical Engineering*. Book Chapter. 1-3:119-134.
9. Gislason MK, Lupidio F, Jónsson HJ, Cristofolini L, Esposito L, Bifulco P, Fraldi M, Gargiulo P. 2020. Three dimensional bone mineral density changes in the femur over 1 year in primary total hip arthroplasty patient. *Clinical Biomechanics*. 78:105092
10. Gargiulo P, Edmunds KJ, Gislason MK, Latour C, Hermannsson P, Esposito L, Bifulco P, Cesarelli M, Fraldi M, Cristofolini L, Jónsson H. 2018. Patient-specific mobility assessment to monitor recovery after total hip arthroplasty. *Proceedings of the Institution of Mechanical Engineers, Part H: Journal of Engineering in Medicine*, 232(10):1048-105.
11. Imam MA, Shehata MSA, Elsehili A, Morsi M, Martin A, Shawqi M, Grubhofer F, Chirodian N, Narvani A, Ernstbrunner L. 2019. Contemporary cemented versus uncemented hemiarthroplasty for the treatment of displaced intracapsular hip fractures: a meta-analysis of forty-two thousand forty-six hips. *International Orthopaedics (SICOT)* 43:1715-1723.
12. Fraldi M, Esposito L, Perrella G, Cutolo A, Cowin SC. 2010. Topological optimization in hip prosthesis design. *Biomech Model Mechanobiol*. 9(4):389-402.
13. Wang X, Xu S, Zhou S, Xu W, Leary M, Choong P, Qian M, Brandt M, Xie YM. 2016. Topological design and additive manufacturing of porous metals for bone scaffolds and orthopaedic implants: A review. *Biomaterials*. 83:127-141.
14. Maji PK, Roychowdhury A, Datta D. 2013. Minimizing stress shielding effect of femoral stem-A review. *J Med Imag Health In*. 3(2):71-178.
15. Ruben RB, Fernandes PR, Folgado J. 2012. On the optimal shape of hip implants. *J Biomech*. 45(2): 239-246.
16. Minutolo V, Esposito L, Sacco E, Fraldi M. 2020. Designing stress for optimizing and toughening truss-like structures. *Meccanica*. 55:1603-1622.
17. Malekmtotie L, Farahmand F, Shodja HM, Samadi-Dooki. 2013 A. An analytical approach to study the intraoperative fractures of femoral shaft during total hip arthroplasty. *J Biomech Eng*. 135(4):041004.
18. Esposito L, Bifulco P, Gargiulo P, Gislason MK, Cesarelli C, Iuppariello L, Jonsson HJ, Cutolo A, Fraldi M. 2018, Towards a patient-specific estimation of intraoperative femoral fracture risk. *Computer Methods in Biomechanics and Biomedical Engineering*. 21(12):663-672.
19. Fraldi M, Cutolo A, Esposito L, D'Amore A. 2016. Visco-elastic and thermal-induced damaging in time-dependent reshaping of human cornea after conductive keratoplasty. *Mech Time-Depend Mater*. 21(1):45-59.
20. Esposito L, Bifulco P, Gargiulo P, Fraldi M. 2015. Singularity-free finite element model of bone through automated voxel-based reconstruction *Comput Methods Biomech Biomed Engin*. 19(3):257-262.
21. Lubliner J. 1990. *Plasticity theory*. MacMillan Publishing. NY.
22. Palladino S, Esposito L, Ferla P, Totaro E, Zona R, Minutolo V. 2020. Experimental and numerical evaluation of residual displacement and ductility in ratcheting and shakedown of an aluminum beam. *Applied Sciences*. 10(10):3610.
23. Morgan EF, Keaveny TM. 2001. Dependence of yield strain of human trabecular bone on anatomic site. *J Biomech*. 34(5):569-577.
24. Kopperdahl DL, Keaveny TM. 1998. Yield strain behavior of trabecular bone *Journal of Biomechanics*. 31:601-608.
25. Ruocco E, Minutolo V. 2012. Two-dimensional stress analysis of multiregion functionally graded materials using a field boundary element model. *Composites Part B: Engineering*. 43(2):663-672.
26. Peng L, Bai J, Zeng X, Zhou Y. 2006. Comparison of isotropic and orthotropic material property assignments on femoral finite element models under two loading conditions, *Medical Engineering & Physics*. 28: 227-233.
27. Keyak JH, Rossi SA, Jones KA, Skinner HB. 1998. Prediction of femoral fracture load using automated finite element modeling *J Biomech*. 31:125-133.
28. Ascenzi MG, Zonca A, Keyak, JH. 2020. Effect of cortical bone micro-structure in fragility fracture patients on lamellar stress. *J Biomech*. 100:109596.
29. Volpe V, Miraglia C, Esposito L, Fraldi M. 2009. X-ray based technique for estimating bone fracture risk. *Proceedings of the 2nd WSEAS International Conference on Biomedical Electronics and Biomedical Informatics*. BEBI '09. 244-246.

30. Katz Y, Yosibash Z, Salai M, Snir N. 2020. Strain shielding for cemented hip implants. *Clin Biomech.* 77:10502.
31. Colombo C, Libonati F, Rinaudo L, Bellazzi M, Ulivieri FM, Vergani L. 2019. A new finite element based parameter to predict bone fracture. *PLoS ONE.* 14(12): e0225905.
32. Schwarzkopf R, Oni JK, Marwin SE. 2013. Total hip arthroplasty periprosthetic femoral fractures: a review of classification and current treatment. *Bull Hosp Jt Dis.* 71(1):68-78.
33. Gruen TA, McNeice GM, Amstutz HC. 1979. "Modes of failure" of cemented stem-type femoral components: a radiographic analysis of loosening. *Clin Orthop.* 141:17-27.
34. Morgan EF, Bayraktar HH, Keaveny TM. 2003. Trabecular bone modulus-density relationships depend on anatomic site. *J Biomech.* 36(7):897-904.